EFFECT OF SURFACE MODIFICATION ON THE CORROSION RESISTIVITY IN SUPERCRITICAL WATER

S. Penttilä[1], A. Horvath[2], A.Toivonen[1] and Z. Zolnai [3]

[1] VTT Technical Research Centre of Finland, Finland

[2] HAS KFKI Atomic Energy Research Institute, Hungary

[3] HAS Research Institute for Technical Physics and Materials Science, Hungary

Abstract

This paper summarizes the results of high temperature corrosion studies of the candidate austenitic alloys at relevant operating conditions for SCWR. The high temperature and pressure above the thermodynamic critical point of water result in higher oxidation rate which might be critical for thin-wall components like fuel cladding. The goal of this work was to study the effect of surface preparation on the oxidation rate on Ti-stabilized austenitic alloy 1.4970. Surfaces were prepared with ion implantation using He^+- and N^+-ions. Samples were immersed in supercritical water at 650°C/25 MPa, for up to 2000 hours. Added to this, conventional surface treatments were conducted for austenitic alloy 316L tube samples in order to study the effect of cold work in sample surface on corrosion resistance. The corrosion rate was evaluated by measuring the weight change of the samples. The compositions of the oxide layers were analyzed using scanning electron microscope (SEM) in conjunction with Energy Dispersive Spectroscopy (EDS).

Keywords: Supercritical water, Austenitic alloy, Oxidation, Surface modification.

1. Introduction

New Generation IV reactor concepts will offer attractive features, but at the same time they also bring new and demanding challenges e.g. for materials technology due to increased operating temperatures and irradiation doses as well as more aggressive coolants and/or longer life time expectations than those of Gen II and Gen III plants. One of the new concepts, sometimes considered as a Gen IV concept and sometimes as an extension of Gen III concepts, is the SCWR (Supercritical Water Reactor). The operating efficiency of water-cooled power plants is largely dependent on the applied temperature and pressure of the system which, are limited by the maximum service parameters of the structural materials. With increasing in-service pressure and temperature, the oxidation resistance of the materials becomes an issue of interest. At the moment, it is not quite clear which materials already licensed for in-core application in nuclear power plants would be useful for thin walled components with regards to the oxidation resistance at the highest design temperatures of the SCWR, although the subject has been studied quite extensively in recent years (e.g. refs. [1-19]).

This work was performed in order to study the effect of some surface modification methods on the oxidation resistance of two austenitic stainless steels.

2. Experimental

2.1 Test materials

Alloy 1.4970 was chosen as one of the base materials of this study due to its historical background, with a lot of data available. The steel has been licensed for use in nuclear power plants and it has been used, for example, in fuel claddings and fuel bundle wrappings of sodium cooled reactors. Alloy 1.4970 is a Ti-stabilized (15% Cr, 15% Ni) austenitic stainless steel. The steel used in this study originates from a hexagonal shaped fuel bundle wrapping and a fuel pin. Thermal treatment of alloy 1.4970 consists of solution annealing at the temperature range of 1050°C and 1120°C and cooling from 900°C to 500°C at the rate of 100°C/min in order to avoid carbide formation at grain boundaries.

The other steel selected for this study is austenitic stainless steel type 316L. This steel has been in extensive use in Gen II and III light water reactors (LWRs). Chemical compositions of the studied alloys are shown in Table 1.

Table 1. Chemical compositions of the studied alloys (W-%).

	C	**Si**	**Mn**	**S**	**P**	**Cr**	**Ni**	**Mo**
316L	0.017	0.36	1.72	0.010	0.028	17.29	13.13	2.52
1.4970	0.095	0.53	1.68	0.001	0.007	15	15.3	1.18
	Cu	**Al**	**W**	**V**	**Ti**	**Co**	**Nb**	**Fe**
316L	-	-	-	-	-	-	-	Balance
1.4970	0.02	0.05	<0.01	0.02	0.45	0.03	-	Balance

2.2 Specimens

Three of the 1.4970 steel specimens were machined from an un-used fuel bundle wrapping to the dimensions of 25 x 15 x 5 mm. One of these specimens was left in the as-machined condition. Two specimens were ground using either #600 or #1200 emery paper. One tubular specimen was cut from an un-used fuel pin. This tubular specimen had the following dimensions: ϕ8 mm, wall thickness 0.6 mm and length 25 mm. The specimen was ground using #1200 emery paper.

Eight 1.4970 specimens, with the same dimensions as the fuel bundle wrapping specimens above, were prepared for ion irradiation. These specimens were ground using #1200 emery paper prior to the irradiations.

Four AISI 316L specimens were prepared from a ϕ10 mm tube used, for example, in the piping of VTT's autoclave laboratory test loops. The wall thickness of the tube samples was 1.5 mm. The length of the samples was approximately 10 mm. One of the samples was left in the as-received state, one was machined, and two of the samples were ground using either #600 or #1200 emery paper.

2.3 Ion irradiations

Multi-step ion irradiation was performed with nitrogen or helium ions in order to create a nearly constant level of damage in a wide depth region of the sample starting from the surface to a depth of about ~1.7 μm for N^+ and ~4.2 μm for He^+ bombardment, respectively, see Fig. 1. The applied ion fluences were estimated with SRIM [20] simulations to create ~1 dpa or ~0.3 dpa damage in the sample. For He^+ bombardment, five irradiation steps were performed, the first two at ion energies of 100 keV and 350 keV perpendicular to the sample surface, and the subsequent steps at 2.5 MeV ion energy at sample tilts of 0^o, 40^o, and 60^o, respectively, see Fig. 1(a). The 3.5 MeV N^+ implantation was done in three subsequent steps at sample tilts of 0^o, 45^o, and 70^o, respectively, as shown in Fig. 1(b). The effect of elements (He and N) on corrosion resistance of alloy 1.4970 is not known at this point. However, helium is presumably distributed into interstitial locations in the matrix but may also form cavities. According to Paszti et al. [21, 22] ion bombardment with light elements at higher energies might result in blistering or flaking of the surface. Also nitrogen is presumably distributed into interstitial locations but may also form nitrides. The selection of a light and a heavy element was considered to investigate the effect of different damage rates in the same corrosion experiment (see Fig. 1.).

The He^+ bombardment at energies of 100 keV and 350 keV was performed with the Heavy Ion Cascade Implanter at the Research Institute for Particle and Nuclear Physics of HAS (MTA RMKI) in Budapest, Hungary. In this case the beam was continuously scanned over the sample surface area of 15 mm × 15 mm.

Ion irradiation with 2.5 MeV He^+ and 3.5 MeV N^+ ions was performed in a sample chamber with a two-axis goniometer connected to the 5 MV EG-2R Van de Graaff accelerator operating at MTA RMKI. The ion beam was collimated with two sets of four-sector slits to the dimensions of X×Y = 2.2 mm × 2 mm. In order to reduce hydrocarbon deposition, liquid N_2 cooled traps were used along the beam path and around the wall of the chamber. The vacuum in the sample chamber was about 10^{-4} Pa. The irradiation of the sample surface area of 15 mm × 15 mm was done by scanning the sample holder with respect to the ion beam, see Fig. 2. For a sample tilt angle of 0^o one scan step is 1.1 mm along the *x* and 1 mm along the *y* direction (half of the beam spot size), therefore a given point of the sample is irradiated 4 times because of the overlapping beam spots. This is done for the homogenization of the fluence within the implanted area. The irradiated charge, i.e. the total number of bombarding particles, was monitored with a transmission Faraday cup. Table 2 comprises all studied 1.4970 samples with different ion implantation treatments. The good thermal conductivity of the sample holder served to stabilize the sample temperature near room temperature. Here *N* denotes nitrogen bombardment, while *He* means helium irradiation.

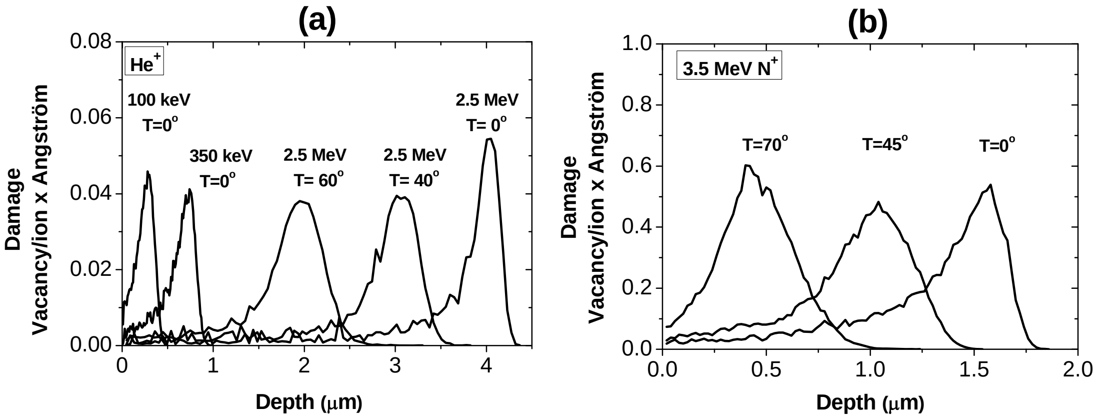

Figure 1. SRIM simulation of damage depth distributions induced by multi-step (a) He^+ and (b) N^+ ion irradiation in stainless steel samples. The ion energy and sample tilt angle are indicated for each irradiation step.

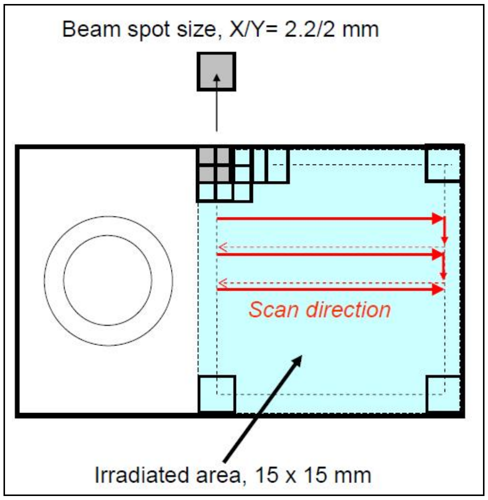

Figure. 2. Schematic of the oxidation test coupon and the Van de Graaff implantation process The irradiated area is indicated with pale blue colour.

Table 2. Details of the multi-step ion irradiation process for eight stainless steel samples. Note that for samples He1, He2, and He3, He4, as well as for N1, N2, and N3, N4 similar implantation treatment has been applied. Ion fluences were chosen to create about 1 dpa (He1, He2, N1, N2) and 0.3 dpa (He3, He4, N3, N4) damage, respectively.

Sample	**Ion**	**Energy (keV)**	**Tilt angle (T)**	**Total fluence (ion/cm^2)**
He1, He2	He$^+$	100	0°	1.2×10^{16}
He3, He4			0°	4×10^{15}
He1, He2	He$^+$	350	0°	1.2×10^{16}
He3, He4			0°	4×10^{15}
He1, He2	He$^+$	2500	0°	2×10^{16}
			40°	2×10^{16}
			60°	2×10^{16}
He3, He4			0°	6×10^{15}
			40°	6×10^{15}
			60°	6×10^{15}
N1, N2	N$^+$	3500	0°	2×10^{15}
			45°	2×10^{15}
			70°	2×10^{15}
N3, N4			0°	6×10^{14}
			45°	6×10^{14}
			70°	6×10^{14}

2.4 Oxidation tests

The specimens were exposed to supercritical water at 650°C/250 bar in a supercritical autoclave connected to a recirculation water loop, Fig. 3a. Temperature, pressure, inlet and outlet water conductivity, dissolved oxygen content and flow rate were monitored and controlled. The monitored test conditions showed that the temperature, pressure, dissolved oxygen, inlet conductivity and outlet conductivity were within the targeted range, Table 3. The samples were attached to a specimen holder rack (Figure 3b). The specimens and the rack were electrically insulated from each other and the autoclave body using ZrO$_2$ washers.

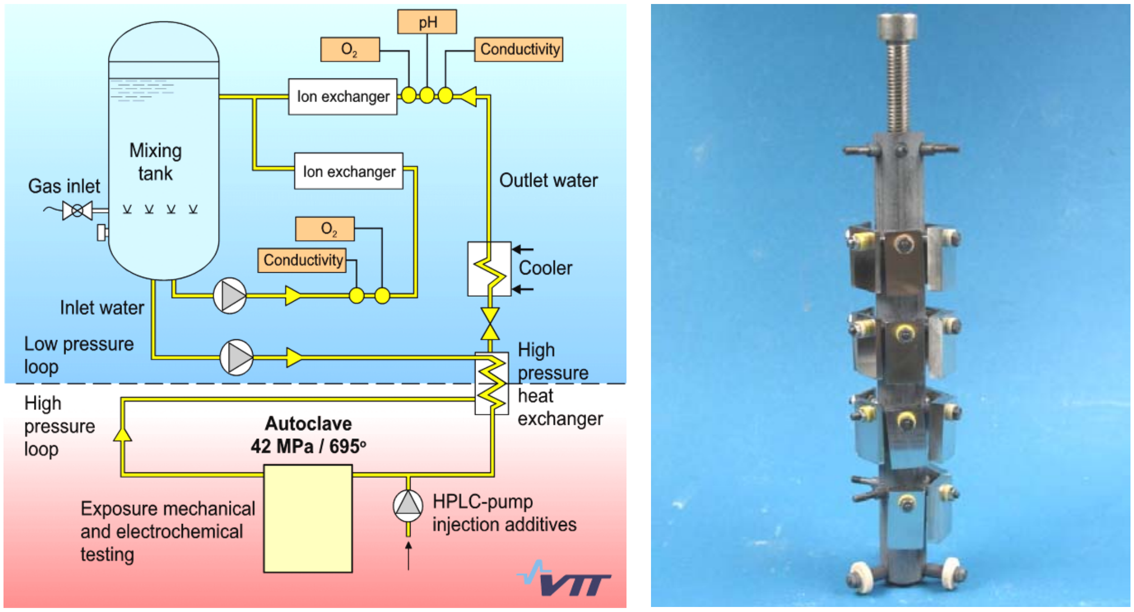

a) b)

Figure 3. a) The supercritical autoclave system at VTT and b) specimen rack with ion implanted test coupons.

Table 3. Targeted and realised values for the test environment.

Quantity	Target value / range	Notes / realised values (mean ± SD)
Temperature	650°C	Recorded mean 649 ± 1.0°C
Pressure	250 bar	Recorded mean 250 ± 0.9 bar
Inlet conductivity	0.1 – 0.5 µS/cm	Recorded mean 0.055 ± 0.001 µS/cm
Outlet conductivity	1.0 – 3.0 µS/cm	Recorded mean 0.30 ± 0.11 µS/cm
Inlet dissolved O_2	150 ppb	Recorded mean 150 ± 0.5 ppb
pH of the inlet water	7.0	(Pure water)
Flow rate	~ 3-5 ml/min	Full renewal about every 4 h

2.5 Post test investigations

The weights of the specimens were measured before and after each test period (1000 h and 2000/3000 h exposures, respectively), and the weight changes per unit area were calculated. After that, metallographic samples were prepared. The oxide layer structures were studied from the cross sections of the metallographic samples using SEM (Scanning Electron Microscopy) and EDS (Energy Dispersive X-ray Spectroscopy).

3. Results and discussion

Figures 4 and 5 summarize the results from weight gain measurements for the tested 1.4970 specimens up to 1000 and 2000 hours of exposure. In general, the tested materials showed a trend of increasing weight gain with time for the 1 dpa specimens, while the effect of 0.3 dpa dose for specimens appear to decrease the weight gain with time within the resolution capability. Generally, the effect of ion implantation was little on the oxidation resistance for the studied samples. This might be due to fact that effect of ion implantation for the specimens could not achieve sufficient defect density under sample surface. For nitrogen implanted samples (samples N1, N2, N3 and N4) the damaged zone extends from the sample surface to a depth of about 1.7 µm, while for helium implanted samples (samples He1, He2, He3 and He4) it is located in the depth range of 0 - 4 µm, respectively. Thus, increased defect density near the sample surface was not adequate to enhance formation of a protective oxide film. The weight gains of all ion implanted 1.4970 samples were smaller than those of mechanically treated samples except for ion implanted sample N3 (0.3 dpa) after 1000 h exposure. The appearance of the 1.4970 specimens are presented in Figures 6 and 7 (He^+ and N^+ implantation respectively) in the as-irradiated and after 2000h of testing, respectively. In all samples, oxide exfoliation is evident. All 1.4970 samples formed a duplex oxide layer in this study consisting an iron-rich outer oxide layer whereas the inner layer contained a significant amount of Cr and Ni. The double layer structure is evident in the SEM-images (and also in EDS-line scans), e.g. for ion implanted sample He4, Figure 8. Table 4 lists the weight changes and oxide thicknesses from SEM-images after 1000 and 2000/3000 h exposure together with 1.4970 and 316L samples with different surface modifications. There is relatively little difference in the observed oxide thickness for the 1.4970 samples. After 2000 h exposure at 650°C, the oxide thicknesses of the ion implanted 1.4970 samples were about 90 – 112 µm. This is approximately 25% of the thickness of the designed cladding wall (0.4 mm) in European HPLWR (High Performance Light Water Reactor) design. Based on observations, thinning of the wall is about the half of the total oxide thickness. So far, no limit has been defined for the wall thickness loss.

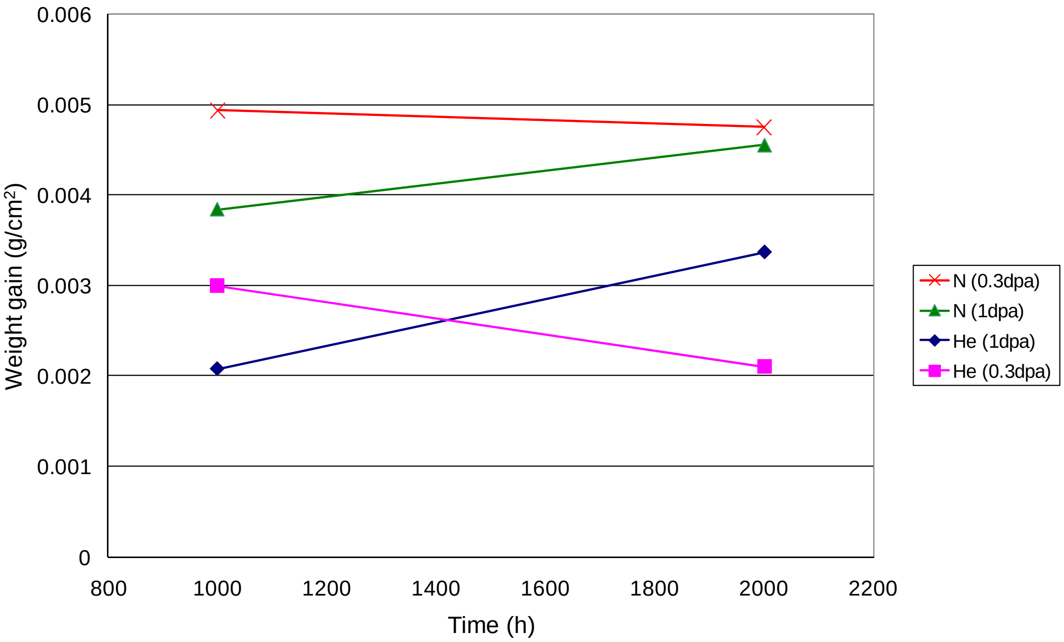

Figure 4. Weight gain of ion-implanted 1.4970 samples (He, N) at 650°C after 1000 and 2000 h exposures.

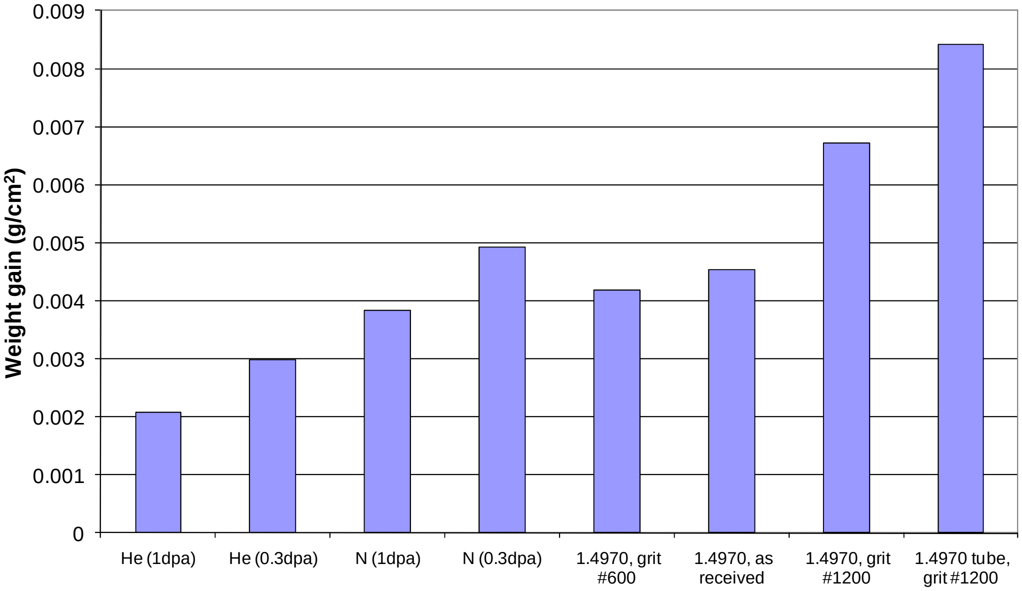

Figure 5. Weight gain of ion-implanted 1.4970 samples (He, N) in comparison with results of mechanically treated 1.4970 samples after 1000 h exposure at 650°C.

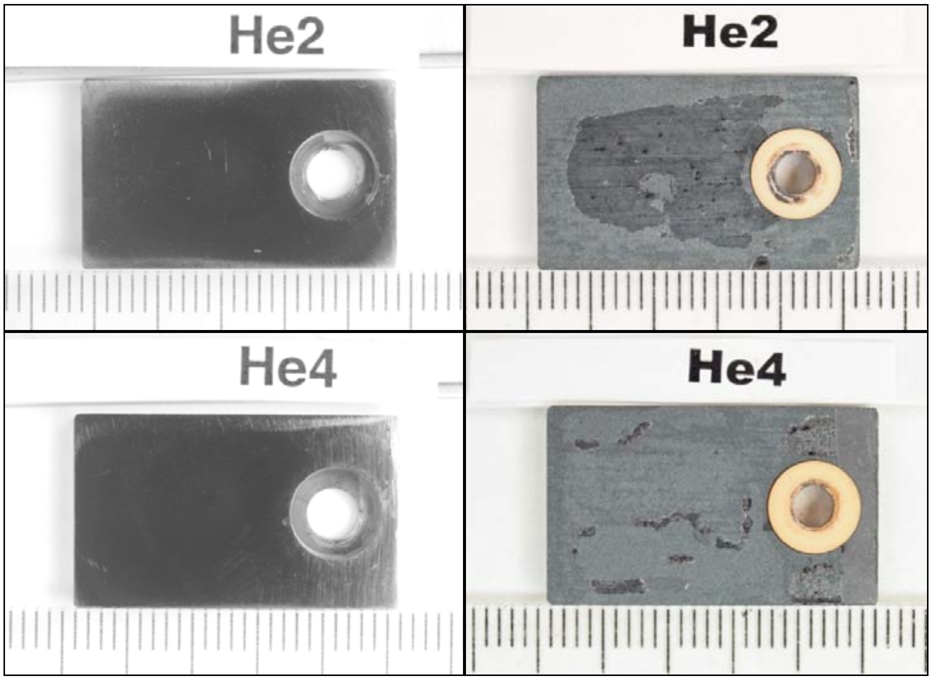

Figure 6. 1.4970 samples with He^+ implantation before (left) and after 2000 h exposure (right) to SCW conditions at 650°C. He2 corresponds to 1dpa and He4 to 0.3dpa doses.

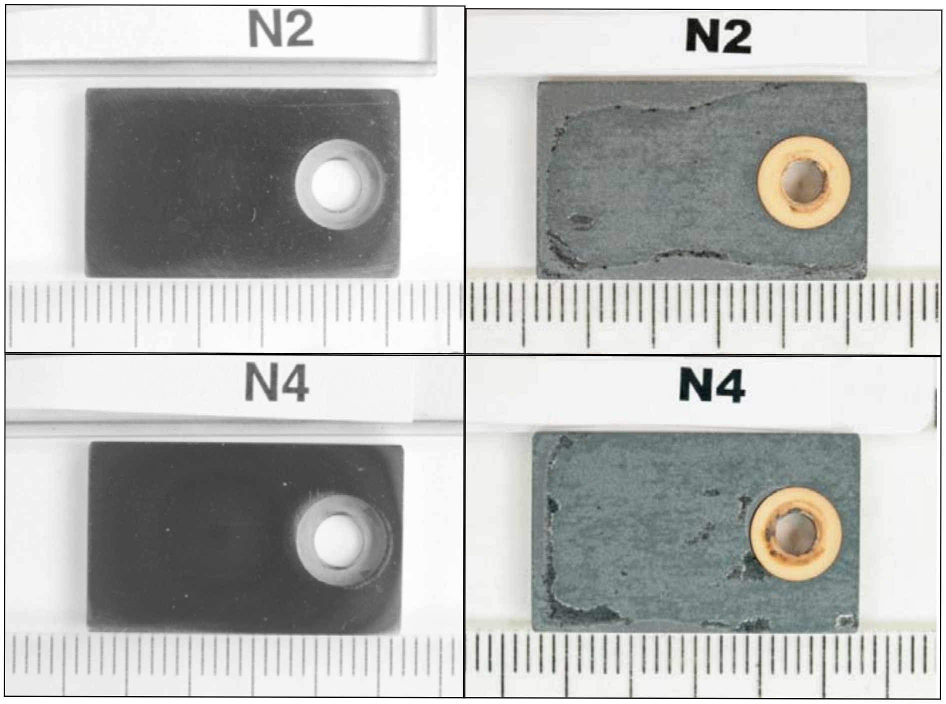

Figure 7. 1.4970 samples with N implantation before (left) and after 2000 h exposure (right) to SCW conditions at 650°C. Note that N2 corresponds to 1dpa and N4 to 0.3dpa doses.

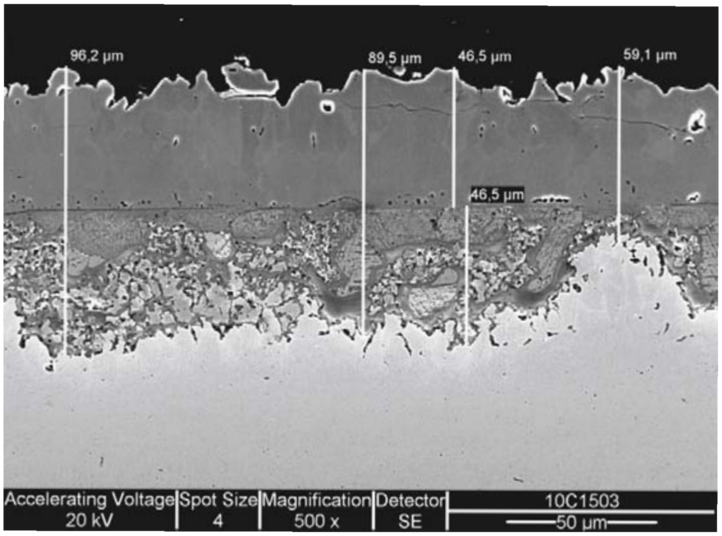

Figure 8. Cross-section SEM-image of ion implanted 1.4970 sample He4 (0.3 dpa) after 2000 h exposure at 650°C

Table 4. Oxide thicknesses and weight changes of modified 1.4970 after 1000 and 2000 h exposures, and mechanically treated 316L tube samples after 1000 h and 3000 h exposures at 650°C (dissolved oxygen 100 – 150 ppb). Oxide thickness at maximum from SEM. n.a. = not available.

Alloy	Surface modification	Oxide thickness and Weight change, 1000h		Oxide thickness and Weight change, 2000h	
1.4970	He (1 dpa)	125 µm	0.00207 g/cm^2	90 µm	0.00337 g/cm^2
1.4970	He (0.3 dpa)	103 µm	0.00299 g/cm^2	96 µm	0.00210 g/cm^2
1.4970	N (1 dpa)	102 µm	0.00383 g/cm^2	112 µm	0.00455 g/cm^2
1.4970	N (0.3 dpa)	89 µm	0.00493 g/cm^2	89 µm	0.00475 g/cm^2
1.4970	machined	118 µm	0.00454 g/cm^2	n.a.	n.a.
1.4970	# 600 emery paper	87 µm	0.00419 g/cm^2	n.a.	n.a.
1.4970	#1200 emery paper	97 µm	0.00672 g/cm^2	n.a.	n.a.
1.4970, tube	#1200 emery paper	96 µm	0.00842 g/cm^2	n.a.	n.a.
Alloy	**Surface modification**	**Oxide thickness and Weight change, 1000h**		**Oxide thickness and Weight change, 3000h**	
316L	machined	2 µm	0.00171 g/cm^2	<1 µm	0.00207 g/cm^2
316L	as received*	50 µm	0.00392 g/cm^2	84 µm	(-) 0.00411 g/cm^2
316L	# 600 emery paper	60 µm	0.00622 g/cm^2	104 µm	(-) 0.00520 g/cm^2
316L	#1200 emery paper	80 µm	0.00582 g/cm^2	81 µm	(-) 0.00518 g/cm^2

*= stock quality

The weight changes of austenitic stainless steel 316L tube samples with different surface finishes (ground with #600 and #1200 emery paper, "as received" (stock quality) condition, and after machining) after 1000 and 3000 h exposure to SCW at 650°C are shown in Fig. 9. The ground specimens (#600 and #1200) and "as received" specimen showed more extensive oxidation than the machined specimen after 1000 h exposure at 650°C. The relative increase in weight gain from 1000 h to 3000 h stopped for the ground and "as received" specimens showing instead of significant weight loses. Machined 316L tube sample showed very little increase in weight gain from 1000 h to 3000 h. A transparent colour of Cr-rich oxide is identifiable even after 3000 h exposure, see Fig 10a. For the machined specimen, it seems that beneficial effect of cold work is sufficient at least up to 3000 h exposure. For other specimens (grit #600 and #1200 and "as received"), a major oxide exfoliation is noticeable after 3000 h exposure, see Figures 10b - 10d. This result was predictable due to fact that such a thick film (50 – 100 µm) is not adherent in cyclic temperature variations. Different thermal conductivities of oxide phases between magnetite and spinel will result internal tensions and might cause scaling of the thick Fe-rich oxide film under SCW conditions [3]. In contrast, the machined 316L sample surface is covered with a continuous, thin and uniform Cr-rich oxide, which led to a relatively small variation in weight gain. The reason for the differences between treatments could be the oxide structure and composition. Thick oxide regions show always an iron rich oxide layer with low chromium concentration in the oxide. On the contrary, machined specimen showed relatively thin (< 1µm) Cr-rich oxide with a peak Cr concentration of about 50% or typically more (depending on location where the line scan has been performed). This is observed in SEM cross-section image and EDS-analysis; see Fig. 11a and Fig. 12, respectively. Based on this study, it is obvious, that different roughness grades of surface treatment result in different degrees of deformation of the surface layer, thus changing the diffusion characteristics of elements in the modified surface layer during exposure to SCW conditions.

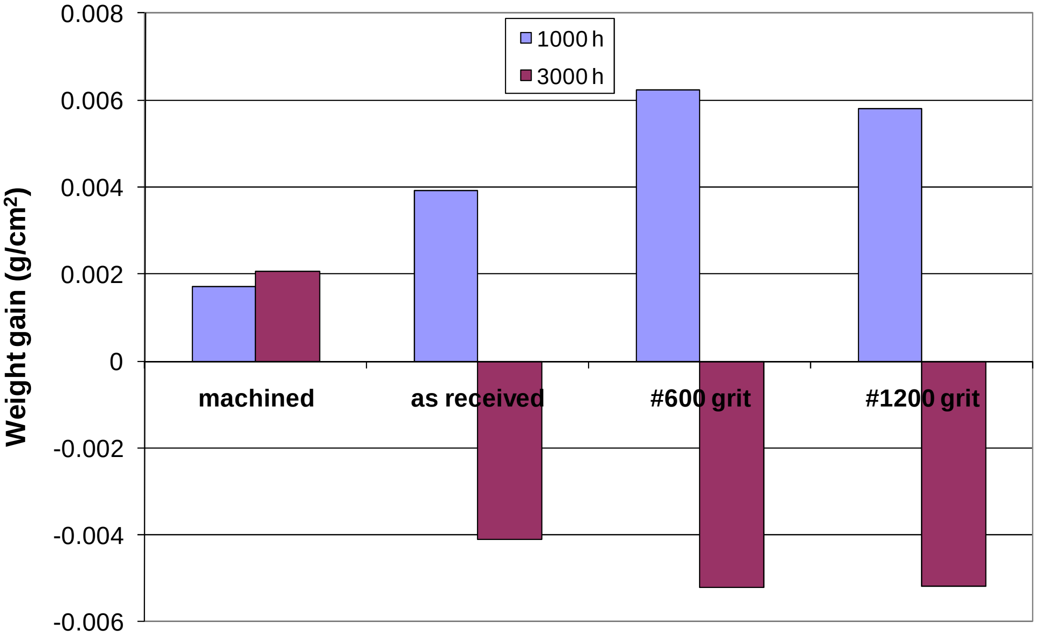

Figure 9. 316L tube samples after 1000 and after 3000 h exposure under SCW at 650°C/25MPa. Note that the total exposure time at 650°C for 316L tube specimens is 3000 h.

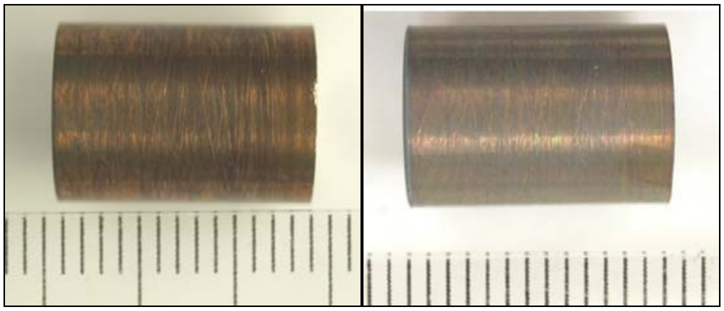

a) 316L tube sample with machined surface before (left, already exposed at 650°C up to 1000 h) and after 3000 h exposure (right) at 650°C.

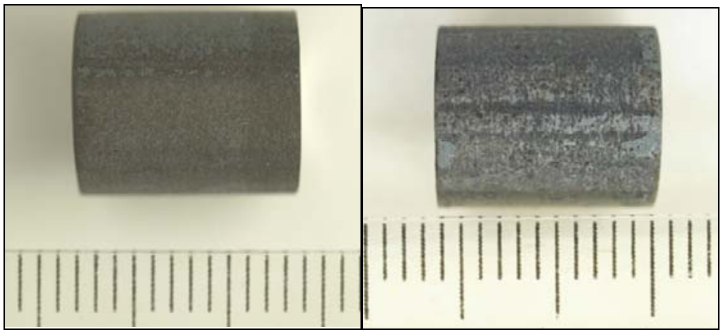

b) 316L tube sample with "as received" surface before (left, already exposed at 650°C up to 1000 h) and after 3000 h exposure (right) at 650°C.

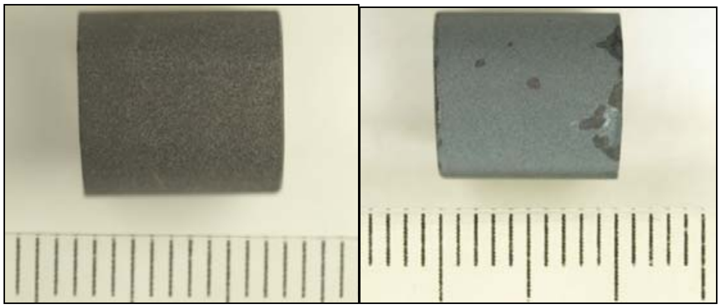

c) 316L tube sample with grit #600 emery paper surface finish before (left, already exposed at 650°C up to 1000 h) and after 3000 h exposure (right) at 650°C.

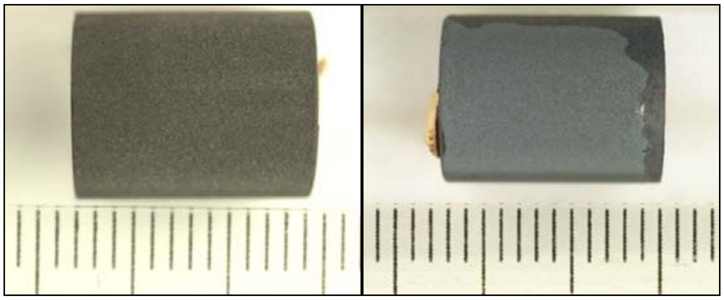

d) 316L tube sample with grit #1200 emery paper surface finish before (left, already exposed at 650°C up to 1000 h) and after 3000 h exposure (right) at 650°C.

Figure 10. Tube samples of austenitic alloy 316L with a) as machined surface, b) with “as received” surface, c) ground with #600 grit emery paper and d) ground with #1200 grit emery paper after the 1000 h and 3000 h exposure to SCW conditions at 650°C (Note that 1000 h exposure was the initial state for the 3000 h exposure test).

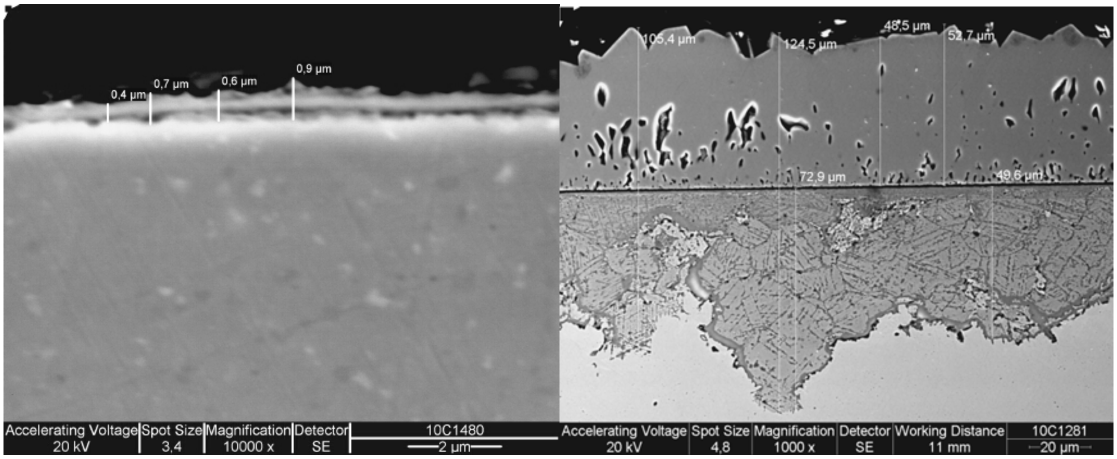

a) b)

Figure 11. Cross-section SEM images after 3000 h exposure at 650°C for 316L tube samples with a) machined and b) with #1200 emery paper finish.

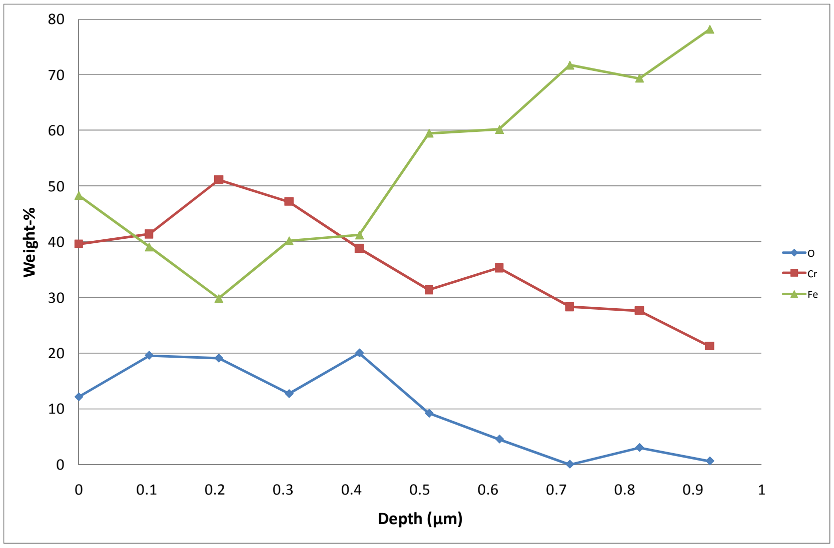

Figure 12. EDS-line scan from cross-section of machined 316L tube sample after 3000h exposure at 650°C.

For ground and “as-received” 316L tube samples a double layer oxide is evident. Fig. 11b shows a double layer oxide on the specimen with the #1200 emery paper finish after 3000 h exposure. The outer layer consists mainly of Fe-rich oxide. This is observed in EDS-analysis performed for 316L tube sample with #1200 emery paper finish, Fig. 13. For ground and “as-received” specimens, Ni and Cr enrichments were observed in the inner oxide layer. Also a small amount of Mn and Mo were observed.

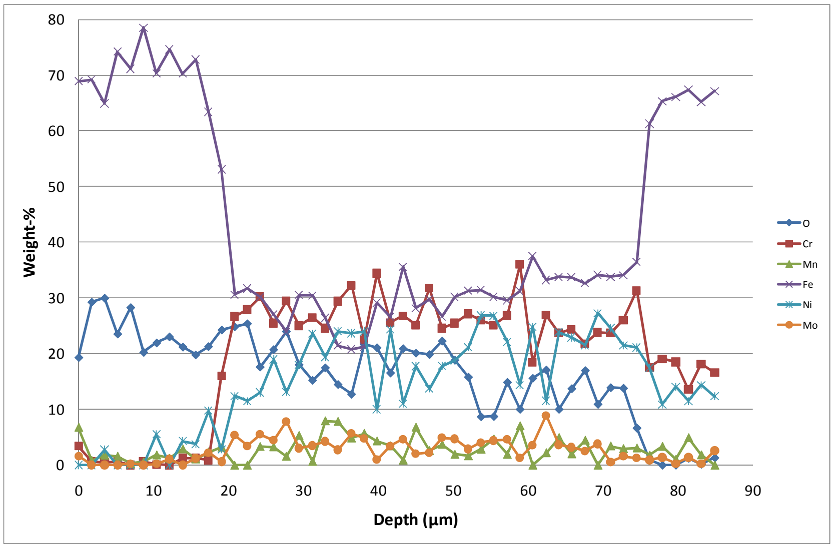

Figure 13. EDS-line scan from cross-section of 316L tube sample with #1200 emery paper finish after 2000h exposure at 650°C.

Typically austenite, magnetite/spinel and hematite phases are observed (by EBSD) for austenitic alloys after SCW exposure. Results of strain distribution studies obtained by

Tan et al. [3] have shown that a strain accumulation close to the interface of ingrown Cr-rich spinel and magnetite layer occurs for alloy 800H in as-received condition, i.e. without grain boundary or surface engineering. This might also be the case in this study for austenitic steels after long term exposure where a thick oxide film has been formed on the sample surface with magnetite as the outer layer and a mixed spinel as the inner layer. Also, significant differences in the thermal expansion coefficients of magnetite and spinel may have led to the sharper strain change at the spinel-magnetite interface on the as-received and ground samples, while the smaller volume thermal expansion coefficient difference between chromia and spinel may have alleviated the strain at the spinel-chromia interface on the machined 316L tube sample. Differences between volume thermal expansion coefficients support the experimental observations that the oxide exfoliation occurred mostly at the spinel-magnetite interface in the as-received and ground samples with a thick magnetite layer. Differences in oxidation resistances between 316L and 1.4970 in machined condition probably results from the Cr and Ni content difference.

Numerous papers in the literature have considered the general corrosion of SCWR candidate materials. Tests have been conducted under wide-ranging conditions, but the temperatures used in experiments have typically been lower than the estimated peak cladding temperature (~620 – 630°C) [1–19]. Based on literature data, the most important variables affecting corrosion behavior of the candidate materials in SCW conditions are alloy class, temperature and surface treatment of the sample surface. Effect of dissolved oxygen content on corrosion resistance is not as significant as expected when the oxygen content is below 300 ppb [17]. However, oxygen content near 300 ppb may limit the total oxide growth as Bartels et al. suggested [18]. In contrast, hydrogen water chemistry (HWC, H_2 30 cc/kg H_2O) used in PWR (Pressurized Water Reactor) plants may not be enough to suppress oxide growth rate of candidate materials in SCW [17]. However, the effect of HWC with much higher H_2 content on oxidation rate is worth to be studied carefully in the near future.

In general, results of this study showed that cold work of a thick surface layer by machining increases the oxidation resistance of 316L under SCW conditions. Shot-peening combined with grain refinement might be the interesting combination due to fact that this has been reported to produce even greater benefit for austenitic alloys (304H and 347HFG), with the resulting oxidation resistance being nearly equivalent to high Cr steels (25% Cr) under USC-conditions (Ultrasupercritical) [19]. Thus, it is recommended that cold-workable materials such as SS 304 are study under SCW conditions as a candidate material. On the other hand, the composition of 1.4970 seems not to be optimal, probably because of its more stable austenitic structure.

4. Conclusions

Surface modifications were performed on austenitic alloy 1.4970 samples by means of ion implantation using He^+- and N^+-ions and mechanical treatments. In addition, selected 316L tube samples with mechanically treated surfaces were exposed at the same time in SCW at 650°C. The effect of different surface modifications on 1.4970 and different conventional surface treatments on 316L tube samples on the oxidation resistance properties were evaluated using weight change measurements and SEM/EDS studies.

Generally, all ion implanted samples were highly oxidized after 2000 h exposure at 650°C. Samples formed a duplex oxide layer, including an iron-rich outer (magnetite) oxide layer and a chromium-rich inner oxide layer with Ni and a certain amount of Mo and Mn. A large iron/oxygen ratio was observed in the outer oxide layer on all samples, indicating high diffusion of iron through the inner oxide layer. The next step following this study could be to adopt chromium ion implantation in order to achieve a Cr-enriched sample surface. It is expected that Cr ion implantation would result in a Cr-rich oxide layer on sample surfaces after exposure to SCW.

Based on this study, thin and apparently protective oxide formed on machined 316L sample at 650°C. The protectiveness lasts at least up to 3000 h. The thin oxide film included a maximum chromium concentration of about 50% (or more) in the oxide. In samples with different treatments, locally thicker oxides had no such Cr-rich peaks in the oxide. In these cases, the oxide remained iron-rich throughout. It should be noted that the tests may not be representative of long-term service in all respects (> 5000 h). In particular, the protective nature of chromium diffusion in cold worked layers could diminish in time, at least in alloys with relatively low Cr content such as in 316L. However, the apparently strong impact of cold working on the early formation of an even Cr-rich oxide can be seen as instructive. This could be significant in a similar way as the usual initial treatment of in-core components to obtain thin and dense protective oxide layers by deliberate pre-oxidation. Such effects are enhanced by the relatively high testing temperature (650°C) in addition to the high dislocation density of cold worked (machined) metal and added diffusion paths resulting from small grain size. The same effect could not be observed on 1.4970. The difference is suspected to be related to the Cr content or the relative Cr and Ni content of the steels.

ACKNOWLEDGEMENTS

We thank the Academy of Finland project NETNUC (New Type Nuclear Reactors) for their financial support.

REFERENCES

[1] S. Penttilä, A. Toivonen, L. Heikinheimo, and R. Novotny, "SCC properties and oxidation behaviour of austenitic alloys at supercritical water conditions", *4th Int. Symposium on Supercritical Water-Cooled Reactors*, 8-11 March, Heidelberg, Germany, Paper No.60, (2009).

[2] S. Penttilä, A. Toivonen, L. Rissanen and L. Heikinheimo, "Generation IV material issues – Case SCWR", *Journal of Disaster Research*, **5** No.4 (2010) 469 – 477.

[3] L. Tan, K. Sridharan, T.R. Allen, R.K. Nanstad, D.A. McClintock, "Microstructure tailoring for property improvements by grain boundary engineering", *Journal of Nuclear Materials*, **374** (2008) 270 – 280.

[4] R. Novotny, P. Hähner, J. Siegl, P. Haušild, S. Ripplinger, S. Penttilä, A.Toivonen, "Stress corrosion cracking susceptibility of austenitic stainless steels in supercritical water conditions", *Journal of Nuclear Materials*, *Article in press* (2010) http://dx.doi.org/10.1016/j.jnucmat.2010.09.018

[5] G. S. Was, T. R. Allen, “Time, temperature, and dissolved oxygen dependence of oxidation in austenitic and ferritic-martensitic alloys in supercritical water”, *Proceedings of ICAPP’05*, Seoul, Korea, paper 5690 (2005).

[6] M. Bojinov, L. Heikinheimo, T. Saario, S. Tuurna, “Characterisation of corrosion films on steels after long-term exposure to simulated supercritical water conditions”, *Proceedings of ICAPP’05*, Seoul, Korea, pp.1799-1807. (2005).

[7] Y. Chen, K. Sridharan, T. R. Allen, S. Ukai, “Microstructural examination of oxide layers formed on an oxide dispersion strengthened ferritic steel exposed to supercritical water”, *Journal of Nuclear Materials*, **359** (2006) 50.

[8] M. Sun, X. Wu, Z. Zhang, E.-H., Han, “Oxidation of 316 stainless steel in supercritical water”, *Corrosion Science*, **51** (2009) 1069 – 1072.

[9] M. Sun, X. Wu, E-H. Han, J. Rao, “Microstructural characterisstics of oxide scales grown on stainless steel exposed to supercritical water”, *Scripta Materialia*, **61** (2009) 996.

[10] Y. Maruno, J. Kaneda, S. Kasahara, N. Saito, T. Shikama and H. Matsui, “Evaluation of weight loss of stainless steels in supercritical water”, *Proceedings of ICAPP’09*, Tokyo, Japan, May 10-14, Paper 9289 (2009).

[11] C. Sun, R. Hui, W. Qu, S. Yick, “Progress in corrosion resistant materials for supercritical water reactors,” *Corrosion Science*, **51**, (2009) 2508 – 2523.

[12] Tsuchiya, Y., Kano, F., Saito, N., Ookawa, M., “Corrosion and SCC properties of fine grain stainless steel in subcritical and supercritical pure water”, *NACE 2007*, Paper 07415.

[13] Teysseyre, S., Was, G., “Stress corrosion cracking of austenitic alloys in supercritical water”, *Corrosion*, **62** No. 12. (2006).

[14] G. S. Was, P. Ampornrat, G. Gupta, S. Teysseyre, E. A. West, T. R. Allen, K. Sridharan, L. Tan, Y. Chen, X. Ren, and C. Pister, “Corrosion and stress corrosion cracking in supercritical water,” *Journal of Nuclear Materials*, **371** (2007) 176 – 201.

[15] Y. Chen, K. Sridharan, T. Allen, “Corrosion of candidate austenitic stainless steels for supercritical water reactors”, *NACE 2007*, Paper 07408. (2007).

[16] Y. Chen, K. Sridharan, S. Ukai, T. Allen, “Oxidation of 9Cr oxide dispersions strengthened steel exposed in supercritical water”, *Journal of Nuclear Materials*, **371** (2007) 118 – 128.

[17] Penttilä, S., Toivonen, A., Heikinheimo, L., Novotny, R., “Corrosion studies of candidate materials for european HPLWR”, *International Congress on Advances in Nuclear Power Plants (ICAPP '08)*, Anaheim, California, USA, June 8 – 12, (2008).

[18] D. M. Bartels, M. Anderson, P. Wilson, T. Allen, K. Sridharan, “Supercritical water radiolysis chemistry - Supercritical water corrosion”, Available on: http://nuclear.inl.gov/deliverables/docs/uwnd_scw_level_ii_sep_2006_v3.pdf

[19] R. Viswanathan, J. Sarver, and J. M. Tanzosh, “Boiler materials for Ultra-Supercritical Coal Power plants - Steamside oxidation,” *Journal of Materials Engineering and Performance*, **15** (2006) 255 – 273.

[20] www.srim.org

[21] F. Pászti, L. Pogány, G. Mezey, E. Kótai, A. Manuaba, L. Pócs, J. Gyulai, T. Lohner, "Investigations on blistering and exfoliation in gold by 3.52 MeV helium ions ", *Journal of Nuclear Materials,* **98** (1981) 11 – 17

[22] F. Pászti, G. Mezey, L. Pogány, M. Fried, A. Manuaba, E. Kótai, T. Lohner and L. Pócs, "Exfoliation on stainless steel and inconel produced by 0.8-4 MeV helium ion bombardment", *Nuclear Instruments and Methods in Physics Research*, **209-210**, Part 2 (1983) 1001-1009